Lipid-Conjugated Rigidochromic Probe Discloses Membrane Alteration in Model Cells of Krabbe Disease

Abbandonato, Gerardo; Storti, Barbara; Tonazzini, Ilaria; Stöckl, Martin; Subramaniam, Vinod; Montis, Costanza; Nifosì, Riccardo; Cecchini, Marco; Signore, Giovanni; Bizzarri, Ranieri

published in
Biophysical Journal
2019

DOI (link to publisher)
10.1016/j.bpj.2018.11.3141

document version
Publisher's PDF, also known as Version of record

Biophysical Journal
Article

Biophysical Society

Lipid-Conjugated Rigidochromic Probe Discloses Membrane Alteration in Model Cells of Krabbe Disease

Gerardo Abbandonato,[1] Barbara Storti,[1] Ilaria Tonazzini,[1] Martin Stöckl,[2] Vinod Subramaniam,[3,4] Costanza Montis,[5] Riccardo Nifosì,[1] Marco Cecchini,[1] Giovanni Signore,[1,6,*] and Ranieri Bizzarri[1,5,*]

[1]NEST, Scuola Normale Superiore and Istituto Nanoscienze CNR (NANO-CNR), Piazza San Silvestro, Pisa, Italy; [2]Bioimaging Center, Department of Biology, Universität Konstanz, Konstanz, Germany; [3]Vrije Universiteit Amsterdam, Amsterdam, The Netherlands; [4]Nanobiophysics, MESA+ Institute for Nanotechnology and MIRA Institute for Biomedical Technology and Technical Medicine, University of Twente, Enschede, The Netherlands; [5]Department of Chemistry and CSGI, University of Florence, Florence, Italy; and [6]Center for Nanotechnology Innovation@NEST, Istituto Italiano di Tecnologia, Pisa, Italy

ABSTRACT The plasma membrane of cells has a complex architecture based on the bidimensional liquid-crystalline bilayer arrangement of phospho- and sphingolipids, which in turn embeds several proteins and is connected to the cytoskeleton. Several studies highlight the spatial membrane organization into more ordered (L_o or lipid raft) and more disordered (L_d) domains. We here report on a fluorescent analog of the green fluorescent protein chromophore that, when conjugated to a phospholipid, enables the quantification of the L_o and L_d domains in living cells on account of its large fluorescence lifetime variation in the two phases. The domain composition is straightforwardly obtained by the phasor approach to confocal fluorescence lifetime imaging, a graphical method that does not require global fitting of the fluorescence decay in every spatial position of the sample. Our imaging strategy was applied to recover the domain composition in human oligodendrocytes at rest and under treatment with galactosylsphingosine (psychosine). Exogenous psychosine administration recapitulates many of the molecular fingerprints of a severe neurological disease, globoid cell leukodystrophy, better known as Krabbe disease. We found out that psychosine progressively destabilizes plasma membrane, as witnessed by a shrinking of the L_o fraction. The unchanged levels of galactosyl ceramidase, i.e., the enzyme lacking in Krabbe disease, upon psychosine treatment suggest that psychosine alters the plasma membrane structure by direct physical effect, as also recently demonstrated in model membranes.

INTRODUCTION

The composition and organization of the plasma membrane (PM) is one of the most debated issues in biophysics, and its description is enriched every year by new biomolecular details. The original fluid mosaic model and the liquid-crystalline interpretation have been overtaken by a spatially interlaced combination of liquid-order (L_o, also referred to as "lipid raft") and liquid-disorder (L_d) phases, enriched respectively in saturated and unsaturated lipids, together with different amounts of cholesterol (1–3). In its simplest description, the "raft" model depicts the PM as a nanostructured dynamic assembly of L_d and L_o phases, which are not separated by definite boundaries but organized around the cytoskeletal network. A continuous exchange of proteins and protein complexes occurs between the two phases, modulated also by the confining action of the cytoskeleton (3). This paradigm of membrane assembly was proposed to be at the basis of and influential in every membrane process, such as formation of protein clusters, signal transduction, endocytosis, and cell polarization and motility (2–6). The raft hypothesis stimulated developments of new techniques for studying the properties and localization of L_o and L_d phases in model and cellular membranes. In this context, fluorescence microscopy offers high sensitivity and low sample perturbation and has become one of the most popular methods (1). Accordingly, in the last few years, the number of published environmentally sensitive fluorescent probes targeted to the membrane has been growing rapidly. These kinds of probes display optical responses able to distinguish L_o and L_d because of the sensitivity to different physicochemical properties of the two phases, such as local polarity (solvatochromic probes) due to hydration and protein presence and/or local viscosity (molecular rotors, also referred to as rigidochromic probes)

Submitted May 25, 2018, and accepted for publication November 16, 2018.

*Correspondence: giovanni.signore@sns.it or r.bizzarri@sns.it

Editor: Joseph Falke.

https://doi.org/10.1016/j.bpj.2018.11.3141

due to lipid packing (7,8). Classical examples of solvatochromic membrane probes are Laurdan (9–12) and Prodan (13), which distribute evenly between L_o and L_d phases, showing strongly blue-shifted emission in the L_o phase of model membranes. Recently, Laurdan was also applied to studies of membrane rafts in live cells, although the data analysis is complicated by the rapid internalization of this dye (14) and the need for two-photon excitation. Other important examples of solvatochromic membrane probes are di-4-ANEPPDHQ and derivates (15), 3-hydroxichromone dyes (i.e., F2N12S (16–18)), coumarins (19), Nile Red, and NR12S derivate (20). On the other hand, most molecular rotors targeted to membrane are functionalized analogs of julolidine (DCVJ, CCVJ) (21,22), BODIPY (23–25), or NBD (26,27). Membrane-targeted rigidochromic probes are widely used to probe the transition from the gel to liquid-crystal phase or, in general, the microviscosity of the phospholipid bilayers (25–28). In most cases, however, available rigidochromic probes targeted to membranes displayed a narrow change of optical properties between the two lipid phases and/or were fairly sensitive to compositional features (e.g., the cholesterol content) as well as changes in local polarity.

Recently, we demonstrated how a close derivative of the green fluorescent protein (GFP) chromophore, **Ge1**, acts as a dual probe of polarity and viscosity, providing fully decoupled fluorescence responses to these parameters (29). In this work, we demonstrate that a lipid bioconjugate of **Ge1**, **Ge1L** (Fig. 1), addresses most drawbacks of membrane-targeted rigidochromic probes, thus offering a reliable means to follow membrane assembly in biochemical studies. Indeed, **Ge1L** is associated with distinct fluorescence lifetimes when embedded in L_o or L_d phases. Such change can be exploited to yield the L_o/L_d composition by phasor analysis of fluorescence lifetime imaging (ph-FLIM), a straightforward approach that relies on a simple graphical analysis of spectral and lifetime fluorescence images when observed in the frequency domain (30–34).

Exploiting its peculiar sensing capabilities, **Ge1L** has been here applied to monitor the remodeling of the PM in a model of Krabbe disease (KD) in vitro. KD (also known as globoid cell leukodystrophy) is a rare, rapidly progressing childhood leukodystrophy triggered by a deficit of the lysosomal enzyme galactosylceramidase (GALC) and characterized by the accumulation of galactosylsphingosine (psychosine; PSY) in the nervous system. Exogenous PSY administrated in vitro to glial cell lines, such as the MO3.13 human oligodendrocytes, is known to recapitulate many of the molecular fingerprints of the disease, including cell death by apoptosis and oxidative stress activation (35). Recently, a few studies showed that the balance between cell membrane rafts and disordered regions are altered in KD cells in vivo and in vitro (36). Dysregulations of pathways related to membrane proteins were also demonstrated by the same group (37). Significantly, our results confirm the progressive membrane alteration of MO3.13 cells upon PSY administration and support the use of **Ge1L** as an imaging tool for further studies in this field.

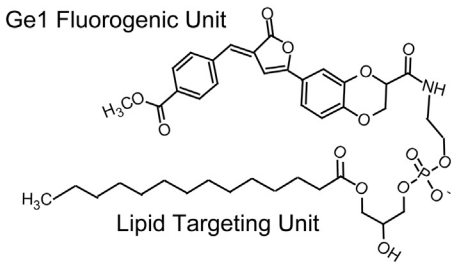

FIGURE 1 Molecular structure of **Ge1L**.

MATERIALS AND METHODS

Materials

1,2-dioleoyl-*sn*-glycero-3-phosphocholine, 1,2-distearoyl-*sn*-glycero-3-phosphocholine, 1,2-dipalmitoyl-*sn*-glycero-3-phosphocholine (DPPC), sphingomyelin, and cholesterol were all from Avanti Polar Lipids (Alabaster, AL). All other reagents were purchased from Sigma Aldrich (St. Louis, MO) (reverse phase grade), and were used without further purification.

Synthetic procedure for Ge1L

The synthetic procedure for **Ge1L** is reported in (38).

Solutions

Details on the preparation of solutions are reported in the Supporting Materials and Methods.

Lipid vesicle preparation

Multilamellar vesicles

A dry lipid film (see below for composition) was prepared from a chloroform solution by evaporation. Homogeneous multilamellar vesicles were prepared by hydrating the lipid film in 20 mM Hepes, 140 mM NaCl (pH 7.4) by vortexing.

Large unilamellar vesicles

The multilamellar vesicles (see above) were subjected to five freeze-thaw cycles (liquid N_2/37°C) before being extruded 11 times through 100 nm polycarbonate filters using a hand-held extruder (Avanti Polar Lipids). Large unilamellar vesicle (LUV) diameters were checked by a Malvern Dynamic Light Scattering system and resulted always in measurements between 100 and 120 nm.

Giant unilamellar vesicles

Giant unilamellar vesicles (GUVs) were prepared through electroformation. Briefly, 10 μL of a 0.5 mg/mL lipid mixture solution in $CHCl_3$ (see below for composition) was deposited on each of two indium tin oxide-coated glass slides on the conductive side. $CHCl_3$ was dried under vacuum

overnight, and a dry lipid film on each sheet was obtained. The electroformation chamber was prepared, sandwiching the sheets with an O-ring separating the lipid films. The chamber was filled with an aqueous solution of sucrose 0.1 M, and the electrical contact between the sheets was provided by putting on each sheet a copper tape connected to a pulse generator, set at a sinusoidal alternating voltage of 10 Hz frequency and two Vpp amplitude for 3 h at 60°C. GUVs were employed within 3 h after preparation.

Compositions of lipid phases

Homogeneous lipid phases were obtained by the following lipid compositions:

L_d: POPC 100% (multilamellar vesicles, LUV, GUV).
L_o: DPPC/cholesterol 70/30 (39) or sphingomyelin/cholesterol/POPC 20/60/20 (40,41) (multilamellar vesicles, LUV).

Nonhomogeneous lipid phases (phase coexistence in vesicles) were obtained by the following lipid compositions:

L_d/L_o: 1,2-distearoyl-*sn*-glycero-3-phosphocholine/1,2-dioleoyl-*sn*-glycero-3-phosphocholine/cholesterol 40/32/28 (GUV) (42).

The chromophore/lipid molar ratio was 1:100 in all experiments.

Cell cultures and treatment

Chinese hamster ovary (CHO) K1 cells were provided by American Type Culture Collection (CCL-61; ATCC, Manassas, VA) and grown in Dulbecco's modified Eagle medium F-12 nutrient mix (DMEM/F-12) supplemented with 10% FBS, 100 U/mL penicillin, and 100 mg/mL streptomycin. All products were from Thermo Fisher (Waltham, MA). For live imaging, 12×10^4 cells were plated 24 h before transfection onto a 35 mm glass-bottom dish (WillCo-dish GWSt-3522; WillCo Beheer B.V., Amsterdam, The Netherlands).

Human oligodendrocyte MO3.13 cells (Cat. No. CLU301-P; Tebu Bio, Le-Perray-en-Yvelines, France) were maintained at 37°C in humidified atmosphere containing 5% CO_2 in high-glucose DMEM supplemented with 2 mM L-glutamine, 1% penicillin/streptomicyn, and 10% heat-inactivated fetal bovine serum (FBS); all products were from Thermo Fisher. For experiments, MO3.13 cells were seeded at 30,000 cells/cm^2 in WillCo dishes, and 24 h after plating, cells were washed two times with phosphate-buffered saline and then cultured in 0.2% FBS medium (DMEM supplemented with 0.2% FBS, 2 mM L-glutamine, and 1% penicillin/streptomicyn). Then, MO3.13 cells were cultured in 0.2% FBS medium (control) or treated with psychosine (PSY) 10 μM for 15 min (PSY15) or for 24 h (PSY24) (35). For selected experiments, cells were also treated with PSY 10 μM for 24 h, then washed and cultured in control 0.2% FBS medium for 6 h (PSY24/6). PSY (Sigma Aldrich) was dissolved in dimethyl sulfoxide; control cultures received the same quantity of dimethyl sulfoxide, which never exceeded 0.1% v/v.

Fluorescence imaging and lifetime measurements

Fluorescence imaging and lifetime measurements were performed by means of a Leica TCS SP5 SMD inverted confocal microscope (Leica Microsystems AG, Buffalo Grove, IL) equipped with an external pulsed diode laser for excitation at 405 and 470 nm and a time-correleated single photon counting acquisition card (PicoHarp 300; PicoQuant, Berlin, Germany) connected to internal spectral detectors. Laser repetition rate was set to 40 Hz. Image size was 256 × 256 pixels, and scan speed was usually set to 400 Hz (lines per second). The pinhole aperture was set to 1.0 Airy. Samples were imaged using a 100 × 1.5 NA oil immersion objective (Leica Microsystems). Emission was monitored in the 480–525 and 540–580 nm ranges, using the built-in acousto-optical beam-splitter detection system of the confocal microscope. Acquisitions lasted until ~100–200 photons per pixel were collected, at a photon-counting rate of 100–500 kHz. The two acquired ranges allowed us to evaluate the generalized poloarization while the lifetime analysis was performed on the joined channels. For each condition, CHO cells (15–20) and MO3.13 cells (30–50) were treated with 1 mg/mL of **Ge1L** in DMEM and imaged after 15 min upon administration at 37°C. At this temperature, **Ge1L** showed negligible internalization by endocytosis for 1 h.

Cholesterol depletion

According to the protocol reported in (43), CHO cells were incubated with 5 mM MβCD at 37°C and 5% CO_2 in the culture medium for different times (1, 2, 3, and 6 h).

GALC level quantification

MO3.13 cells were plated on standard six-well plates, treated as previously reported, and lysed on ice by 120 μL/well of radioimmunoprecipitation assay (R0278; Sigma Aldrich), containing protease and phosphatase inhibitors cocktail (cOmplete and PhosSTOP; Roche Diagnostics, Basel, Switzerland). Cell lysates were centrifugated (15000 × g for 15 min, 4°C), and then the supernatants were tested for protein concentration by a protein assay kit (Micro BCA, Pierce; Thermo Scientific). 10 μL of each sample (on average, 10 μg of protein lysate was used per assay) was tested for GALC assay. The GALC assay was performed with specific synthetic fluorescent 6-hexadecanoylamino-4-methylumbelliferyl-β-D-galactopyranoside (HMU) following procedures previously described (44). Briefly, we performed the assay by mixing 10 μL of protein extract (10–15 μg) with 20 μL of 50 μM HMU substrate (freshly suspended in 0.2 M Na_2HPO_4/0.1M citric-acid buffer (pH 5.2) with 0.02% w/v of sodium azide). Reactions were incubated 17 h at 37°C and then stopped with 0.2 M glycine/NaOH-buffer (pH 10.7) with 0.2% Na-dodecylsulfate (170 μL). After stopping the assay, 100 μL aliquots from the total solution were transferred to 96-well plates for reading in a fluorescence plate reader (GloMax multiplate reader; Promega, Madison, WI) at the wavelengths of HMU (emission filter: 415–485 nm; excitation filter: ultraviolet 365 nm). Each lysate was run in duplicate. Results were normalized for protein content and reported in % with respect to control condition.

Statistical analysis on L_o of MO3.13

L_o fractions in MO3.13 are reported as average value ± the standard error of the mean (mean ± standard error), obtained from $n \geq 3$ independent experiments. Data were statistically analyzed by GraphPad PRISM 5.00 program (GraphPad Software; San Diego, CA). One-Way ANOVA (Dunnett's multiple comparison test) analysis was used; the mean values obtained in each repeated experiment were assumed to be normally distributed about the true mean. Statistical significance refers to results where $p < 0.05$ was obtained.

Molecular dynamics simulations

Two different compositions of the lipid bilayer were simulated, one L_d with 1-palmitoyl-2-oleoyl-*sn*-glycero-3-phosphocholin (POPC) as a model of the disordered phase, the other L_o with DPPC and cholesterol (70:30) as a model of the ordered phase. The starting configurations for the lipid bilayer patches were obtained using the Membrane Builder at the Charmm-Gui website (www.charmm-gui.org). Each leaflet of system L_d contained 38 POPC molecules, whereas that of system L_o contained 13 cholesterol and 32 DPPC molecules. The systems were solvated in a box of water molecules (4435 in system L_d and 3626 in system L_o), and

Na^+/Cl^- ions were added (corresponding to NaCl concentration of 0.2 M) within the usual periodic boundary condition scheme. The Charmm36 force field was used for the lipids in the bilayer and for the lipid tail of the **Ge1L**. The TIP3P model was used for water molecules. For the chromophore part, the charges and other force field parameters were adjusted starting from those of Reuter et al. for the GFP chromophore (45) and from those suggested by CgenFF (46) available online (https://cgenff.umaryland.edu/). Some specific torsion angle parameters were reparameterized by comparison with QM-MP2 scans. Gromacs (47) was used to run the molecular dynamics simulations (version 5.0.5). The simulations were performed using a 2 fs time step, with constraints on the bond lengths by the LINCS algorithm. A constant temperature (310 K) and pressure (one bar) ensemble was forced by, respectively, the v-rescale thermostat (with separate thermostats for water and the rest of the system) and the Parrinello-Rahman barostat (or Berendsen in the initial equilibration stages) with semi-isotropic pressure coupling, in which changes in the z direction are uncoupled to those in the x-y plane, as appropriate for lipid bilayer systems. Temperature and pressure time couplings were 0.2 and 5.0 ps, respectively. The Verlet cutoff scheme was used, with a 1.2 nm cutoff for van der Waal's and Coulomb short-range interactions. The long-range Coulomb interactions were treated with the usual particle mesh Ewald scheme. The **Ge1L** molecule was added to the solvent part of the system. The lipid bilayers were partially denatured by increasing the temperature to 450 K for 10 ns and then letting the system gradually cool down to 310 K. This automatically led to the insertion of the molecule into the lipid bilayer. The systems were then simulated for 300 ns. The average surface area of the simulated lipid bilayer patches was 23.8 (0.6) nm^2 for system L_d and 18.4 (0.2) nm^2 for system L_o. Extending the simulations up to 500 ns did not result in any relevant change to the results shown.

RESULTS

Spectroscopic properties of Ge1L in solution and in LUVs

At first, the spectroscopic properties of **Ge1L** were evaluated in solvents and solvent mixtures with different polarities and viscosities. In the visible range of the electromagnetic spectrum, the absorption spectrum of **Ge1L** peaks around 419 nm and displays poor dependence on the solvent polarity (Table 1). Conversely, the fluorescence emission ranges between 497 and 521 nm (Table 1), depending on the dielectric properties of the solvent (38). The fluorescence decay of **Ge1L** is biexponential (Table 1), in keeping with the peculiar emission photophysics of its fluorogenic unit **Ge1** that entails two concurring excited states (29). Yet, time-resolved anisotropy measurements in tetrahydrofurane (THF) show a rotational correlation time (θ) of ~200 ps, much longer than expected for untargeted **Ge1** (1–10 ps). This finding suggests that in **Ge1L**, the lipid tether somewhat restrains the rotational degrees of freedom of the fluorogenic unit. The strong rigidochromism of **Ge1L** is witnessed by the double-logarithmic lifetime versus viscosity (Förster-Hoffman (48,49)) linear plot obtained in mixtures of variable viscosity (Fig. 2 *b*).

Next, the spectral and rigidochromic properties of **Ge1L** were investigated in LUVs of 100 nm diameter. LUVs are classical in vitro models of cell membrane phases and are frequently used to validate membrane probes (1,41). LUVs were tested to investigate the optical response of **Ge1L** in pure lipid environments, namely the L_d and L_o phases (see Materials and Methods). Note that lipid compositions leading to homogeneous phases were carefully selected in all cases, following (39,40). We observed that the phase nature negligibly affects the spectral emission properties of **Ge1L**. This complies with the similar dielectric properties explored by **Ge1L** in the bilayer. Instead, embedding the probe into the rigid bilayer environment leads to rather long fluorescent lifetimes, still biexponential

TABLE 1 Spectroscopic Properties of Ge1L in Solvents and Lipid Phases

Solvent	ε^a	$\lambda_{abs,max}$ (nm)	$\lambda_{em,max}$ (nm)	η (cP)	τ_1 (ns)	τ_2 (ns)	% τ_1
CCl_4	3.2	420.5	497	0.91	2.21	1.22	60
AcOEt	3.3	416.5	508	0.42	2.42	1.14	25
THF	2.7	420	507	0.48	1.71	0.97	61
IPA	2.4	420	518	2.06	1.85	0.75	13
MeOH	2.6	416	521	0.59	2.30	0.78	12
L_o	–	–	512	–	3.67	2.15	46
L_d	–	–	519	–	6.20	3.20	75

[a]Molar extinction coefficient (*10^{+4}).

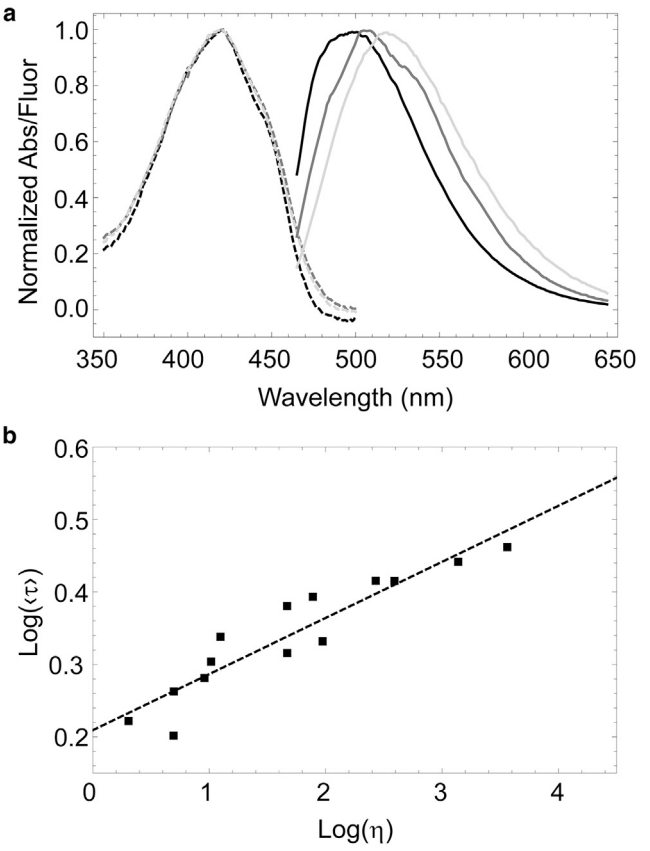

FIGURE 2 Spectroscopic properties of **Ge1L** in solvents and solvent mixtures with variable polarity and viscosity. (*a*) Absorption (*dashed*) and emission (*full*) spectra in CCl4 (*black*), THF (*gray*), and isopropryl alcohol (IPA, *light gray*). (*b*) Forster-Hoffmann plot: $\log(\langle\tau\rangle)$ vs. $\log(\eta)$ of **Ge1L** in Triton X-100/isoamyl alcohol, THF/PEG400, and CCl_4/polybutene mixtures.

in nature (Table 1). Remarkably, however, **Ge1L** average lifetimes differ by more than 3 ns between the L_d and L_o domains (Table 1). This finding indicates that the intramolecular twisting of **Ge1L** is much more hampered in L_o than in L_d phases. Dynamic anisotropy measurements support this picture because we measured $\tau = 15$ ns in L_d domains and $\tau > 100$ ns in L_o domains, in both cases with the same intrinsic anisotropy $r_0 = 0.34$. For comparison, $r_0 = 0.35$ in THF, demonstrating that the nature of the medium does not affect the transition dipole moments of **Ge1L**.

The emission properties of **Ge1L** were also assessed in GUVs either characterized by homogeneous L_d phase or L_d/L_o phase coexistence (42). Fluorescence analysis indicated that **Ge1L** is much more emissive in L_o, with a relative intensity ratio $r = I(L_d)/I(L_o) = 0.18 \pm 0.01$. Such an intensity ratio can be expressed by

$$r = \frac{I(L_d)}{I(L_o)} = \frac{\varepsilon(L_d)}{\varepsilon(L_o)} \times \frac{\Phi(L_d)}{\Phi(L_o)} \times K_p, \qquad (1)$$

where ε stands for the extinction coefficient, Φ for the quantum yield, and K_p is the partition ratio [**Ge1L** (L_d)]/[**Ge1L** (L_o)].

On account of the poor sensitivity of **Ge1L** absorption to the local environment, we can assume that $\varepsilon(L_d)/\varepsilon(L_o) \cong 1$. Also, the ratio of quantum yields can be expressed by the ratio of average lifetimes $\Phi(L_d)/\Phi(L_o) \cong \tau(L_d)/\tau(L_o) = 0.52$, under the reasonable hypothesis that the radiative lifetime is negligibly affected by the lipid environment. This leads to $K_p = 0.35$, i.e., **Ge1L** partitions more preferably in L_o phase than in L_d, likely on account of the saturated structure of its lipid tether.

Molecular dynamics simulations

Molecular dynamics simulations of the **Ge1L**/LUV system shed light over the observed rigidochromic behavior of the probe in the L_d and L_o domains. In L_d domains, the fluorogenic unit of **Ge1L** positions approximately parallel to the lipid-water interface, and its center of mass is localized, on average, at 0.8 nm underneath (Fig. 3 *a*).

Additionally, the amplitude of the distributions clearly indicates some flexibility of the fluorogenic unit inside the bilayer. Conversely, in L_o domains, the chromophore "kernel" slips down into the bilayer (the average position of the center of mass is 1.4 nm below the polar phosphate heads) and is characterized by poor flexibility (Fig. 3 *b*). Notably, in L_o domains, the cholesterol molecules accumulate near the fluorogenic unit: the interaction with the hydroxyl group of cholesterol could explain the slightly higher dielectric constant detected in L_o as compared to L_d domains ($\varepsilon = 15$–16 in L_o vs. $\varepsilon = 8$–10 in L_d domains) (38). The different flexibility of the fluorophore is also confirmed by the dihedral angle distributions of both its phenyl groups Phe1 and Phe2 (scheme 1), which in L_o regions show sharp peaks at 0 and 180°, respectively (Fig. S1, *a* and *b*). Conversely, in the L_d phase, only a slight bias appears between their orientations. In this case, the steric effect of the "flagpole" hydrogen is more evident. Finally, the obtained flip-flop frequencies (Fig. S1 *c*) are Phe1(L_o) = 0.00 ns^{-1}, Phe1(L_d) = 0.04 ns^{-1}, Phe2(L_o) = 0.01 ns^{-1}, and Phe2(L_d) = 0.28 ns^{-1}. These findings attest that although the Phe1 is mostly blocked by the steric hindrance of the targeting lipid, Phe2 is very sensitive to the different phase orders.

ph-FLIM and membrane domain composition in CHO

The strong sensitivity of **Ge1L** lifetime to the nature of the lipid phase prompted us to evaluate ph-FLIM (30) as a convenient means to spatially map the phase composition in cell membranes. The phasor analysis represents, in a polar two-dimensional plot ("phasor plot" (50)), the cosine ($g_{i,j}$) and sine ($s_{i,j}$) Fourier transforms of the normalized emission decay collected in each pixel i, j of an image. For monoexponential decays, the phasor ($g_{i,j}$, $s_{i,j}$) lies on a semicircle (universal circle) of radius 1/2 and center (1/2, 0); for multiexponential decays, the phasor lies inside the

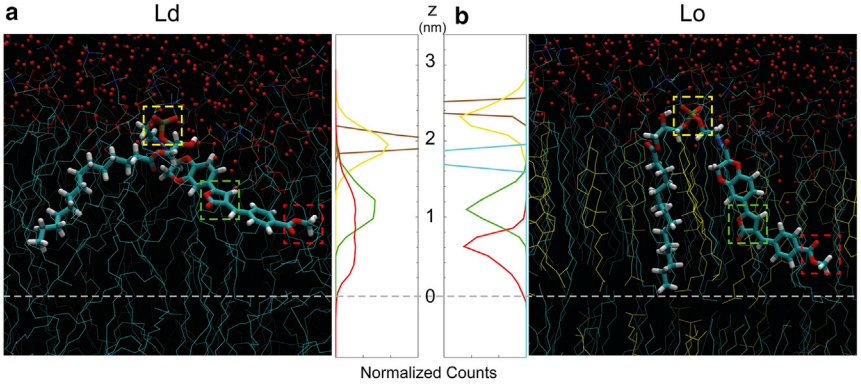

FIGURE 3 Molecular dynamics of L_d or L_o homogeneous lipid bilayers embedding **Ge1L**. (*a*) On the left, a representative snapshot of molecular dynamics simulations of **Ge1L** interacting with L_d phase; on the right, a histogram reporting the depth within the bilayer of the lipid phosphate groups (*brown*), the **Ge1L** phosphate head (*yellow*), the imidazolinone ring (*green*), and the carboxymethyl molecular tether (*red*) is shown. (*b*) Same as for (*a*) but relevant to L_o phase (note that the snapshot is on the *right* and the depth histogram on the *left*). In light blue is the cholesterol hydoxyl distribution. To see this figure in color, go online.

semicircle. On the phasor plot, the combinations of distinguishable photophysical states, such as those determined by L_d and L_o phases, follow a vectorial addition rule, regardless of the number of exponentials they entail (30,50,51). Thus, the individual contributions of lipid phases to a given membrane location can be quantified by simple vector algebra starting from the reference phasors relevant to L_d and L_o domains. To calibrate ph-FLIM, we obtained the reference phasors by ph-FLIM of **Ge1L** embedded in multilamellar vesicles characterized by homogeneous L_d or L_o phases. The finite precision of our measurements and/or the vesicle heterogeneity pinpointed a phasor distribution for each phase whose mass center was taken as the reference value (Fig. 4).

After calibration, **Ge1L** was put to the test to quantify the phase domains of the PM of CHO cells. First, a colocalization experiment between the marker $DiIC_{18}(5)$-DS and **Ge1L** confirmed that our probe selectively stains the PM of the living cells (Fig. S2). Next, we carried out FLIM and ph-FLIM analysis. The average lifetime of **Ge1L** in the PM of CHO cells is ~4.2 ns. Comparison of this value with the lifetimes found in L_o and L_d phases (Table 1) suggests the "interlaced" coexistence of the two domains, as hypothesized for the modern model of the PM. Accordingly, ph-FLIM highlighted a phasor cloud lying on the calibration line that connects the L_o and L_d phases (Fig. S3). Vector algebra led to fractional intensity compositions (i.e., the fraction of emitted photons by **Ge1L** in each phase) $\chi(L_o) = 60\%$ and $\chi(L_d) = 40\%$. This result is in good agreement with data obtained by other dyes such as Laurdan (52).

The relative abundances $f(L_o)$ and $f(L_d)$ of the two phases were calculated from the intensity ratio r, according to

$$f(L_o) = \frac{r \times \chi(L_o)}{1 + r \times \chi(L_o) - \chi(L_o)}; f(L_d) = 1 - f(L_o). \quad (2)$$

We found out $f(L_o) = 21\%$ and $f(L_d) = 79\%$.

Cholesterol depletion of the PM was reflected in a significant shift of the phasor cloud in the plot (Fig. 5), in excellent agreement with the expected gradual disappearance of the ordered phase (20,43).

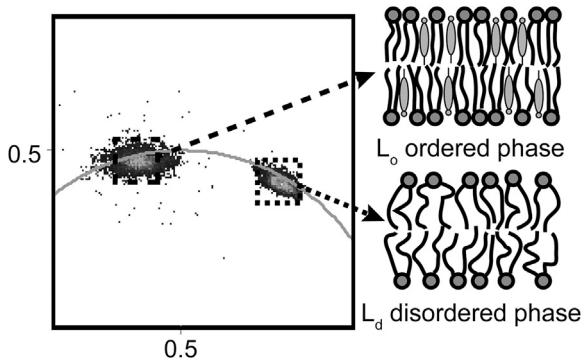

FIGURE 4 Phasor plot of **Ge1L** in multilamellar vesicles whose compositions enable the homogeneous L_d or L_o phases.

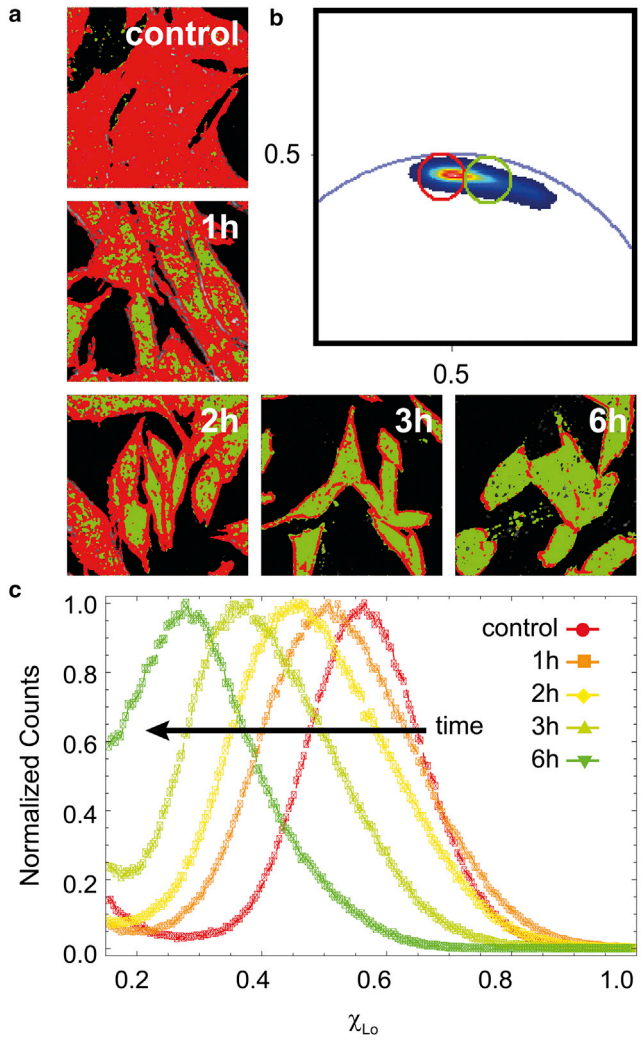

FIGURE 5 ph-FLIM of **Ge1L** in the PM of CHO cells. (*a*) Temporal evolution of the cholesterol depletion observed through **Ge1L** lifetime. The colors of the images in panel (*a*) are relative to the phasor plot (*b*). The histograms in (*c*) describe the trend of the calculated intensity fraction of **Ge1L** in L_o phase during the extraction process (from *red* to *green*: control, 1, 2, 3, and 6 h). To see this figure in color, go online.

Membrane domain composition in MO3.13 oligodendrocytes

We then applied **Ge1L** to study the PM in a model of KD in vitro. MO3.13 human oligodendrocyte cells were cultured in control conditions or treated with PSY 10μM (35,53) for different times: 15 min (PSY15), 24 h (PSY24), or 24 h followed by a 6 h recovery in control conditions (PSY24/6). In all conditions, the membrane L_o/L_d ratio was measured by ph-FLIM using **Ge1L**.

The exposure to PSY induced a linearly decreasing trend in fraction of L_o phase (Fig. 6 *a*) as compared to control.

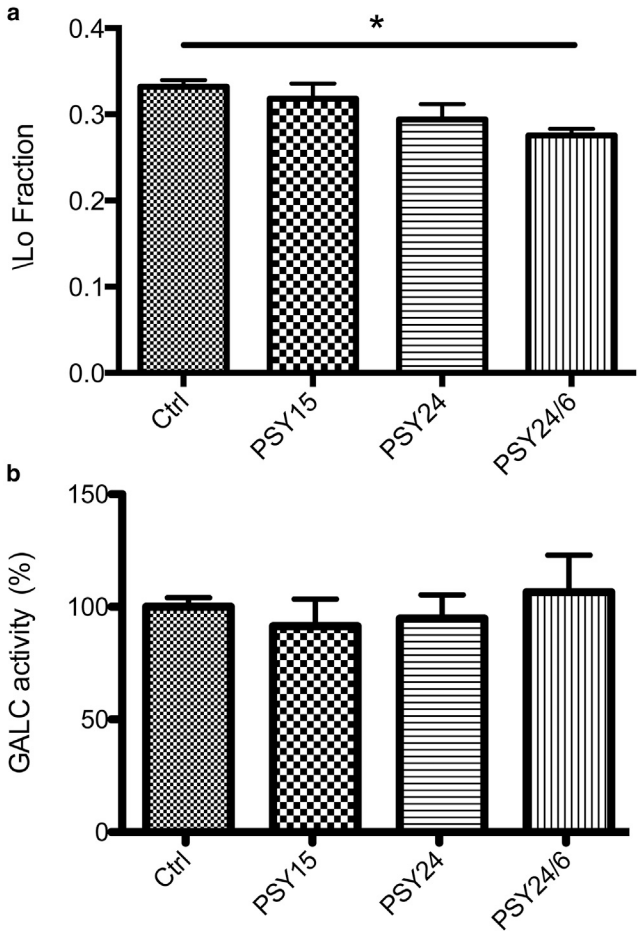

FIGURE 6 (*a*) Quantification of L_o domain in cell membrane by **Ge1L**. Mo3.13 cells were cultured in control conditions or treated with PSY 10 μM for 15 min (PSY15), 24 h (PSY24), or 24 h followed by a 6 h recovery in control conditions (PSY24/6). *$p < 0.05$ control vs. PSY24/6, one-way ANOVA Dunnett's test. (*b*) Level of GALC activity in MO3.13 cells in different conditions (*as above*). The GALC assay was performed with HMU, and results are reported in % in respect to control condition. In all cases, error bars refer to 1 SD.

This behavior was visible in all the experiments (single data sets are reported in Fig. S4). Notably, the presence of PSY in the medium at the measurement time enhances cell variability, as witnessed by the larger SDs detected for PSY15 and PSY24. Removal of PSY in PSY24/6 diminishes cell variability, and the depletion of the L_o phase due to PSY exposure becomes statistically significant ($p < 0.05$ vs. control, one-way ANOVA, Dunnett's test). Concomitantly to ph-FLIM, we measured the level of the GALC enzyme (i.e., the enzyme lacking in KD) in parallel batches of MO3.13 cells treated in the same ways to verify whether the change in membrane order was correlated to GALC activity. Our findings highlight that GALC activity is stable in the treated and untreated cells (Fig. 6 *b*). These data suggest that GALC enzyme activity is not affected by the destabilization of the PM in MO3.13 cells induced by PSY.

DISCUSSION

Fluorescence is a highly dynamic phenomenon occurring in the ns timescale. This relatively long time window allows for the occurrence of several processes that can strongly modify the nature of emission, including nanoscale friction by surrounding molecules (rigidochromism). **Ge1L** is a lipid bioconjugate of an efficient and polarity-independent rigidochromic probe, **Ge1**, which targets selectively the PM of living cells. In the modern picture of the PM, the coexistence of ordered and disordered domains appears to be behind a variety of processes, such as formation of protein clusters, signal transduction, endocytosis, cell polarization, and motility (54). Accordingly, the detection of membrane phase composition is a relevant target in biophysics (1). We found that **Ge1L** partitions in both L_d and L_o phases, in which it experiences rather different environments in terms of local fluidity, as witnessed by a large change in fluorescence lifetime. Our molecular dynamics simulations afford a rational explanation for this phenomenon: **Ge1L** pins deeply inside the bilayer in L_o domains, whereupon it experiences a very rigid environment. Conversely, the higher molecular flexibity experienced by **Ge1L** in L_d phases is owed to the closer position of the fluorogenic unit to the lipid bilayer surface.

The large lifetime difference of **Ge1L** in lipid bilayers identifies two "reference states" that can be usefully exploited by ph-FLIM (31,33). From these reference states and the relative intensities of the dye therein, the simple vectorial rules of ph-FLIM enable the straightforward determination of the fractions of L_d and L_o phases in each single pixel after **Ge1L** imaging. When **Ge1L** stains the cell membrane, ph-FLIM measurement of L_d and L_o fractions is a suitable way to construct a map of cell membrane composition. We note that the typical diffraction-limit resolution of a wide-field fluorescence or confocal microscope operating with visible light is, at most, around 200 nm. This means that the lifetime from each pixel reflects an average of L_d and L_o phases, whose dimensions were identified below 50 nm by several authors (3,55,56), although this figure is still a matter of debate, and the actual value is unknown. Notably, Kuimova et al. proposed the same ph-FLIM approach for a different molecular rotor, although they did not provide a quantitative estimate of the two phases in living cells (57,58).

It is worth noting that the homogeneous lipid systems used to calibrate L_d and L_o phases in ph-FLIM are simplistic representations of the actual L_d and L_o nanophases in cells, which both contain proteins, cholesterol, variable amounts of charged lipids, and other biomolecules. Yet, for calibration, we need a stable model system in which we know, for sure, that we have homogeneous ("pure") phases. Anything closer to the real lipid composition already may introduce nanodomains. Giant PM vesicles, for example, show phase separation, but this does not show up in the lifetime

histogram, as previously reported by some of us (27). As previously stated, our phasor calibration method identifies two pure "states" and predicts that any mixture of these two states would fall along their connection line in the phasor plot. Remarkably, phasors of **Ge1L** in cell membrane do fall along this line, substantiating the strong effect on lifetime by the local phase composition. However, this does not imply that the two ideal states are actually there, but rather that we can interpret the composition in any membrane point as ideally made up of two limit pure phases. Actually, the strength of ph-FLIM applied to **Ge1L** resides in our capability to relate membrane changes to real composition shifts toward one or the other of the two pure phases, yielding a biological insight. Our experiments on cells attest to that.

At first, **Ge1L** was simply applied to analyze the membrane of reference CHO cells. There, we found out that the L_o phase accounts for ~21% of the recorded intensity, and this fraction is critically dependent on the available cholesterol. In more biologically insightful experiments, **Ge1L** highlighted the membrane alteration in MO3.13 human oligodendrocyte provoked by PSY, the cytotoxic sphingolipid that accumulates in the nervous system in KD owing to loss of GALC activity. Data reported in Fig. 6, along with the single experiment data sets (Fig. S4), show that PSY administration to MO3.13 cells destabilizes the membrane, supported by the rather large variation of phase compositions measured when the cells are exposed and imaged in the presence of PSY. Importantly, our findings reveal the shrinking of the L_o phase along with PSY exposure. This decrease is partially hidden by data variability for PSY15 and PSY24 conditions, but it becomes statistically significant when PSY is removed after 24 h of exposure and cells are allowed to recover for 6 h (PSY24/6). Additionally, PSY effect seems unrelated to GALC activity, thus excluding a feedback action of PSY-induced membrane alteration against the accumulation of PSY. The latter data suggest that prolonged exposure to PSY might induce irreversible alterations in the PM, far beyond the possibility of rescue by endogenous GALC.

The PM changes upon PSY treatment were recently addressed by biochemical means. In all cases, PSY was found to induce significant lipid raft alteration and slight enrichment of cholesterol (36,37,59). Significantly, the non-natural enantiomer of PSY (*ent*-PSY) was found to have equal or greater toxicity compared with PSY (60). This strongly suggests that PSY exerts its toxic action through a nonenantioselective mechanism, possibly through membrane perturbation rather than through stereospecific protein-PSY interactions. In keeping with this hypothesis, Diaz et al. very recently reported that PSY remodels physically model lipid membranes at neutral pH (61). Actually, they found out that PSY reduces the compactness of the membrane and increases the fraction of the disordered phase.

The in cellulo reduction of L_o phases that we observed upon PSY administration fits very well in this context, representing the first proof, to our knowledge, of the physical action of PSY on actual PM. Our findings, also, are not contradictory with the reduction of lateral mobility observed by some authors in the myelin membrane upon PSY treatment (36). Indeed, PSY intercalation in the ordered domains leads to the loss of several raft proteins (e.g., caveolin-1) that are apparently displaced by the toxic lipid. **Ge1L** could be forced out of the altered ordered domains, signaling the shrinking of the L_o phase. At any rate, our experimental results add new insights into this puzzling scenario, directly linking the previous observations about KD raft composition alteration to a physical property of the membrane, which we could directly measure thanks to the **Ge1L** probe.

CONCLUSIONS

We here reported on a fluorescent analog of the GFP chromophore that, when conjugated to a phospholipid, enables the quantification of the L_o and L_d domains in living cells on account of its large fluorescence lifetime variation in the two phases. The lifetime variation stems from a different rigidochromic effect on the fluorogenic unit of **Ge1L** due to the dissimilar arrangement of the probe in L_o and L_d domains, as demonstrated by molecular dynamics simulations. We note that spatially resolved quantification of L_o and L_d domains is a relevant goal in fluorescence microscopy of living cells on account of the regulating role of the two bilayer phases on several biological processes. Indeed, many approaches have been proposed to achieve this goal. The advantage of our **Ge1L** probe lies in the combination of excitation and emission in the visible range of electromagnetic spectrum (for instance, the popular membrane probe Laurdan requires ultraviolet or two-photon excitation), with high sensitivity to the two phases by a rigidochromic effect on its lifetime. Additionally, the use of ph-FLIM leads to a straightforward, all-graphic determination of L_o and L_d composition in each pixel. Our imaging strategy was applied to unveil the effect of PSY administration to human oligodendrocytes, a simple in vitro model of KD that nonetheless recapitulates most of the molecular phenotypes associated with this pathology. We observed that PSY progressively destabilizes the PM, as witnessed by a shrinking of the L_o fraction. The unchanged levels of GALC, i.e., the enzyme lacking in KD, upon PSY treatment suggest that PSY alters the PM structure by a direct physical effect, possibly without altering the lipid metabolism of the cell. This confirms experiments by Hawkins-Salsbury et al. (60) that highlighted similar membrane destabilization effects by PSY and its non-natural enantiomer that are not recognized by the stereospecific cell machinery. We believe that **Ge1L** represents a, to our knowledge, novel remarkable molecular fluorescent indicator to monitor, with

sub-micrometer spatial resolution, any biological process that leads to membrane remodeling and/or destabilization.

SUPPORTING MATERIAL

Supporting Materials and Methods and four figures are available at http://www.biophysj.org/biophysj/supplemental/S0006-3495(18)34509-0.

AUTHOR CONTRIBUTIONS

G.A., M.S., R.N., M.C., G.S., and R.B. designed research. G.A., B.S., I.T., M.S., R.N., G.S., and R.B. performed research. G.A., I.T., R.N., M.C., G.S., and R.B. analyzed data. All authors wrote the manuscript.

ACKNOWLEDGMENTS

The authors acknowledge Prof. Piet Dijkstra (Twente University) for useful discussions.

This research was supported by 1) Regione Toscana, Bando Fondo Aree Sottoutilizzate Salute 2014, under the framework of the project "DIAMANTE-Diagnostica Molecolare Innovativa per la scelta terapeutica personalizzata dell'adenocarcinoma pancreatico" (grant number CUP I56D15000310005); 2) Fondazione Cassa Di Risparmio di Lucca, under the framework of the project "Pre-Clinical Testing of Lithium Treatment in Krabbe Disease"; 3) European Leukodystrophy Association (ELA) International, under the framework of the project "Development of a novel, nanovector-mediated enzyme replacement therapy for Globoid Cell Leukodystrophy (GLD)", grant no. ELA 2015-010C1A.

REFERENCES

1. Klymchenko, A. S., and R. Kreder. 2014. Fluorescent probes for lipid rafts: from model membranes to living cells. *Chem. Biol.* 21:97–113.
2. Jacobson, K., O. G. Mouritsen, and R. G. Anderson. 2007. Lipid rafts: at a crossroad between cell biology and physics. *Nat. Cell Biol.* 9:7–14.
3. Lingwood, D., and K. Simons. 2010. Lipid rafts as a membrane-organizing principle. *Science.* 327:46–50.
4. Simons, K., and E. Ikonen. 1997. Functional rafts in cell membranes. *Nature.* 387:569–572.
5. Brown, D. A., and E. London. 2000. Structure and function of sphingolipid- and cholesterol-rich membrane rafts. *J. Biol. Chem.* 275:17221–17224.
6. Simons, K., and D. Toomre. 2000. Lipid rafts and signal transduction. *Nat. Rev. Mol. Cell Biol.* 1:31–39.
7. M'Baye, G., Y. Mély, …, A. S. Klymchenko. 2008. Liquid ordered and gel phases of lipid bilayers: fluorescent probes reveal close fluidity but different hydration. *Biophys. J.* 95:1217–1225.
8. Haidekker, M. A., T. P. Brady, …, E. A. Theodorakis. 2005. Effects of solvent polarity and solvent viscosity on the fluorescent properties of molecular rotors and related probes. *Bioorg. Chem.* 33:415–425.
9. Parasassi, T., G. De Stasio, …, E. Gratton. 1990. Phase fluctuation in phospholipid membranes revealed by Laurdan fluorescence. *Biophys. J.* 57:1179–1186.
10. Parasassi, T., M. Di Stefano, …, E. Gratton. 1992. Membrane aging during cell growth ascertained by Laurdan generalized polarization. *Exp. Cell Res.* 202:432–439.
11. Harris, F. M., K. B. Best, and J. D. Bell. 2002. Use of laurdan fluorescence intensity and polarization to distinguish between changes in membrane fluidity and phospholipid order. *Biochim. Biophys. Acta.* 1565:123–128.
12. Gaus, K., T. Zech, and T. Harder. 2006. Visualizing membrane microdomains by Laurdan 2-photon microscopy. *Mol. Membr. Biol.* 23:41–48.
13. Rottenberg, H. 1992. Probing the interactions of alcohols with biological membranes with the fluorescent probe Prodan. *Biochemistry.* 31:9473–9481.
14. Owen, D. M., C. Rentero, …, K. Gaus. 2011. Quantitative imaging of membrane lipid order in cells and organisms. *Nat. Protoc.* 7:24–35.
15. Kwiatek, J. M., D. M. Owen, …, K. Gaus. 2013. Characterization of a new series of fluorescent probes for imaging membrane order. *PLoS One.* 8:e52960.
16. Demchenko, A. P., Y. Mély, …, A. S. Klymchenko. 2009. Monitoring biophysical properties of lipid membranes by environment-sensitive fluorescent probes. *Biophys. J.* 96:3461–3470.
17. Klymchenko, A. S., and A. P. Demchenko. 2002. Electrochromic modulation of excited-state intramolecular proton transfer: the new principle in design of fluorescence sensors. *J. Am. Chem. Soc.* 124:12372–12379.
18. Oncul, S., A. S. Klymchenko, …, Y. Mély. 2010. Liquid ordered phase in cell membranes evidenced by a hydration-sensitive probe: effects of cholesterol depletion and apoptosis. *Biochim. Biophys. Acta.* 1798:1436–1443.
19. Signore, G., R. Nifosì, …, R. Bizzarri. 2009. A novel coumarin fluorescent sensor to probe polarity around biomolecules. *J. Biomed. Nanotechnol.* 5:722–729.
20. Kucherak, O. A., S. Oncul, …, A. S. Klymchenko. 2010. Switchable nile red-based probe for cholesterol and lipid order at the outer leaflet of biomembranes. *J. Am. Chem. Soc.* 132:4907–4916.
21. Haidekker, M. A., and E. A. Theodorakis. 2007. Molecular rotors–fluorescent biosensors for viscosity and flow. *Org. Biomol. Chem.* 5:1669–1678.
22. Sutharsan, J., D. Lichlyter, …, E. A. Theodorakis. 2010. Molecular rotors: synthesis and evaluation as viscosity sensors. *Tetrahedron.* 66:2582–2588.
23. Kuimova, M. K. 2012. Mapping viscosity in cells using molecular rotors. *Phys. Chem. Chem. Phys.* 14:12671–12686.
24. Kuimova, M. K., G. Yahioglu, …, K. Suhling. 2008. Molecular rotor measures viscosity of live cells via fluorescence lifetime imaging. *J. Am. Chem. Soc.* 130:6672–6673.
25. López-Duarte, I., T. T. Vu, …, M. K. Kuimova. 2014. A molecular rotor for measuring viscosity in plasma membranes of live cells. *Chem. Commun. (Camb.).* 50:5282–5284.
26. Stöckl, M., A. P. Plazzo, …, A. Herrmann. 2008. Detection of lipid domains in model and cell membranes by fluorescence lifetime imaging microscopy of fluorescent lipid analogues. *J. Biol. Chem.* 283:30828–30837.
27. Stöckl, M. T., and A. Herrmann. 2010. Detection of lipid domains in model and cell membranes by fluorescence lifetime imaging microscopy. *Biochim. Biophys. Acta.* 1798:1444–1456.
28. Nipper, M. E., S. Majd, …, M. A. Haidekker. 2008. Characterization of changes in the viscosity of lipid membranes with the molecular rotor FCVJ. *Biochim. Biophys. Acta.* 1778:1148–1153.
29. Abbandonato, G., D. Polli, …, R. Bizzarri. 2018. Simultaneous detection of local polarizability and viscosity by a single fluorescent probe in cells. *Biophys. J.* 114:2212–2220.
30. Digman, M. A., V. R. Caiolfa, …, E. Gratton. 2008. The phasor approach to fluorescence lifetime imaging analysis. *Biophys. J.* 94:L14–L16.
31. Battisti, A., M. A. Digman, …, R. Bizzarri. 2012. Intracellular pH measurements made simple by fluorescent protein probes and the phasor approach to fluorescence lifetime imaging. *Chem. Commun. (Camb.).* 48:5127–5129.
32. Battisti, A., S. Panettieri, …, R. Bizzarri. 2013. Imaging intracellular viscosity by a new molecular rotor suitable for phasor analysis of fluorescence lifetime. *Anal. Bioanal. Chem.* 405:6223–6233.

33. Ferri, G., L. Nucara, …, R. Bizzarri. 2016. Organization of inner cellular components as reported by a viscosity-sensitive fluorescent Bodipy probe suitable for phasor approach to FLIM. *Biophys. Chem.* 208:17–25.

34. Koenig, M., B. Storti, …, G. Bottari. 2016. A fluorescent molecular rotor showing vapochromism, aggregation-induced emission, and environmental sensing in living cells. *J. Mater. Chem. C.* 4:3018–3027.

35. Del Grosso, A., S. Antonini, …, M. Cecchini. 2016. Lithium improves cell viability in psychosine-treated MO3.13 human oligodendrocyte cell line via autophagy activation. *J. Neurosci. Res.* 94:1246–1260.

36. D'Auria, L., C. Reiter, …, E. R. Bongarzone. 2017. Psychosine enhances the shedding of membrane microvesicles: implications in demyelination in Krabbe's disease. *PLoS One.* 12:e0178103.

37. White, A. B., F. Galbiati, …, E. R. Bongarzone. 2011. Persistence of psychosine in brain lipid rafts is a limiting factor in the therapeutic recovery of a mouse model for Krabbe disease. *J. Neurosci. Res.* 89:352–364.

38. Signore, G., G. Abbandonato, …, R. Bizzarri. 2013. Imaging the static dielectric constant in vitro and in living cells by a bioconjugable GFP chromophore analog. *Chem. Commun. (Camb.).* 49:1723–1725.

39. Veatch, S. L., and S. L. Keller. 2003. Separation of liquid phases in giant vesicles of ternary mixtures of phospholipids and cholesterol. *Biophys. J.* 85:3074–3083.

40. Smith, A. K., and J. H. Freed. 2009. Determination of tie-line fields for coexisting lipid phases: an ESR study. *J. Phys. Chem. B.* 113:3957–3971.

41. Wu, Y., M. Stefl, …, M. K. Kuimova. 2013. Molecular rheometry: direct determination of viscosity in Lo and Ld lipid phases via fluorescence lifetime imaging. *Phys. Chem. Chem. Phys.* 15:14986–14993.

42. Montis, C., V. Generini, …, D. Berti. 2018. Model lipid bilayers mimic non-specific interactions of gold nanoparticles with macrophage plasma membranes. *J. Colloid Interface Sci.* 516:284–294.

43. Zidovetzki, R., and I. Levitan. 2007. Use of cyclodextrins to manipulate plasma membrane cholesterol content: evidence, misconceptions and control strategies. *Biochim. Biophys. Acta.* 1768:1311–1324.

44. Ribbens, J. J., A. B. Moser, …, G. H. B. Maegawa. 2014. Characterization and application of a disease-cell model for a neurodegenerative lysosomal disease. *Mol. Genet. Metab.* 111:172–183.

45. Reuter, N., H. Lin, and W. Thiel. 2002. Green fluorescent proteins: empirical force field for the neutral and deprotonated forms of the chromophore. Molecular dynamics simulations of the wild type and S65T mutant. *J. Phys. Chem. B.* 106:6310–6321.

46. Vanommeslaeghe, K., E. Hatcher, …, A. D. Mackerell, Jr. 2010. CHARMM general force field: a force field for drug-like molecules compatible with the CHARMM all-atom additive biological force fields. *J. Comput. Chem.* 31:671–690.

47. Hess, B., C. Kutzner, …, E. Lindahl. 2008. GROMACS 4: algorithms for highly efficient, load-balanced, and scalable molecular simulation. *J. Chem. Theory Comput.* 4:435–447.

48. Forster, T., and G. Hoffmann. 1971. Viscosity dependence of fluorescent quantum yields of some dye systems. *Zeitschrift Fur Physikalische Chemie-Frankfurt.* 75:63.

49. Haidekker, M. A., and E. A. Theodorakis. 2010. Environment-sensitive behavior of fluorescent molecular rotors. *J. Biol. Eng.* 4:11.

50. Clayton, A. H., Q. S. Hanley, and P. J. Verveer. 2004. Graphical representation and multicomponent analysis of single-frequency fluorescence lifetime imaging microscopy data. *J. Microsc.* 213:1–5.

51. Hirshfield, K. M., D. Toptygin, …, L. Brand. 1993. Dynamic fluorescence measurements of two-state systems: applications to calcium-chelating probes. *Anal. Biochem.* 209:209–218.

52. Owen, D. M., D. J. Williamson, …, K. Gaus. 2012. Sub-resolution lipid domains exist in the plasma membrane and regulate protein diffusion and distribution. *Nat Commun.* 3:1256.

53. Voccoli, V., I. Tonazzini, …, M. Cecchini. 2014. Role of extracellular calcium and mitochondrial oxygen species in psychosine-induced oligodendrocyte cell death. *Cell Death Dis.* 5:e1529.

54. Simons, K., and M. J. Gerl. 2010. Revitalizing membrane rafts: new tools and insights. *Nat. Rev. Mol. Cell Biol.* 11:688–699.

55. Kusumi, A., K. G. Suzuki, …, T. K. Fujiwara. 2011. Hierarchical mesoscale domain organization of the plasma membrane. *Trends Biochem. Sci.* 36:604–615.

56. Owen, D. M., and K. Gaus. 2013. Imaging lipid domains in cell membranes: the advent of super-resolution fluorescence microscopy. *Front. Plant Sci.* 4:503.

57. Dent, M. R., I. López-Duarte, …, M. K. Kuimova. 2016. Imaging plasma membrane phase behaviour in live cells using a thiophene-based molecular rotor. *Chem. Commun. (Camb.).* 52:13269–13272.

58. Sherin, P. S., I. López-Duarte, …, M. K. Kuimova. 2017. Visualising the membrane viscosity of porcine eye lens cells using molecular rotors. *Chem. Sci. (Camb.).* 8:3523–3528.

59. White, A. B., M. I. Givogri, …, E. R. Bongarzone. 2009. Psychosine accumulates in membrane microdomains in the brain of krabbe patients, disrupting the raft architecture. *J. Neurosci.* 29:6068–6077.

60. Hawkins-Salsbury, J. A., A. R. Parameswar, …, M. S. Sands. 2013. Psychosine, the cytotoxic sphingolipid that accumulates in globoid cell leukodystrophy, alters membrane architecture. *J. Lipid Res.* 54:3303–3311.

61. Zulueta Díaz, Y. L. M., S. Caby, …, M. L. Fanani. 2018. Psychosine remodels model lipid membranes at neutral pH. *Biochim. Biophys. Acta Biomembr.* 1860:2515–2526.